Supplemental Material :
Understanding the warp in free ⟨111⟩ metal nanowires by modeling surface elasticity

Marc Gailhanou and Jean-Marc Roussel
Aix Marseille Université, CNRS, IM2NP UMR 7334, 13397, Marseille, France

In this supplementary material, we detail how the bulk elastic parameters C_{ij} and the surface elastic parameters C^S_{ij} vary with the azimuth Θ in the geometry encountered in a ⟨111⟩ wire of circular cross-section. The Θ dependence of C_{ij} and C^S_{ij} are determined for copper and for gold by performing Molecular Statics (MS) calculations with the SMA potential. Expressions of the deformation state of the wire characterized by u_0, w_0 and $g(R,\Theta)$ are derived. Warp displacement fields obtained in ⟨111⟩ Cu nanowires are shown for two different cross-sections (circular or hexagonal with {112} surfaces). Finally, we show that in the case of ⟨111⟩ Au nanowires with triangular cross-sections, the surface shear stress is responsible for the twist of the wires.

I. BULK ELASTIC CONSTANTS

In the framework of the linear elasticity, the bulk energy density $\psi(\mathbf{E})$ depends only on the second order elastic constants C_{ij} where i and j range over the values 1,2, ...,6 in the Voigt's convention. Strain changes the 6 components S_i of the symmetric bulk stress $\mathbf{S}$ according to

$$S_i = C_{ij} E_j \tag{1}$$

using Einstein summation convention and Brugger notation[1] to identify the components in cylindrical coordinates: $S_1 = S_{RR}$, $S_2 = S_{\Theta\Theta}$, $S_3 = S_{ZZ}$, $S_4 = S_{\Theta Z}$, $S_5 = S_{RZ}$, $S_6 = S_{R\Theta}$, and $E_1 = E_{RR}$, $E_2 = E_{\Theta\Theta}$, $E_3 = E_{ZZ}$, $E_4 = 2E_{\Theta Z}$, $E_5 = 2E_{RZ}$, $E_6 = 2E_{R\Theta}$. In a reference frame rotating with the angle Θ around a ⟨111⟩ direction, only

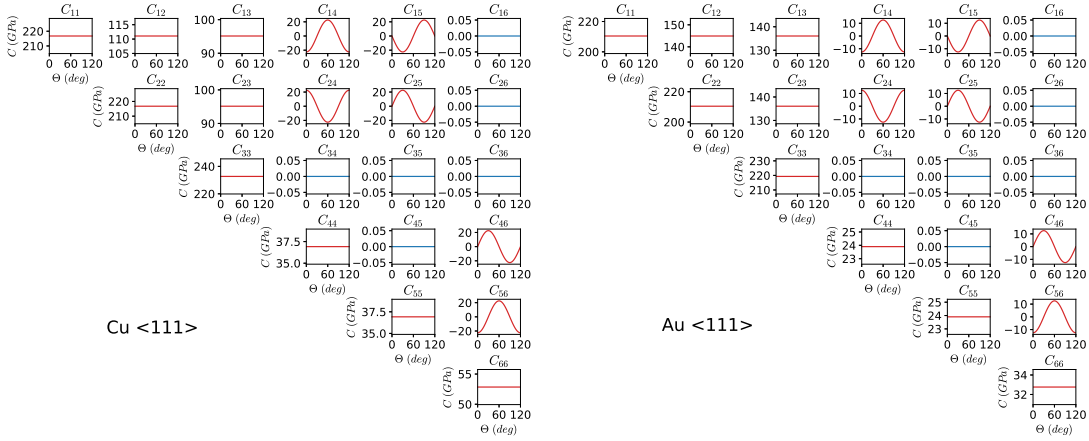

FIG. 1. Dependence with the azimuth Θ of the bulk elastic constants C_{ij} for copper (matrix on the left) and for gold (matrix on the right) in a reference frame rotating with the angle Θ around a ⟨111⟩ direction, according to Eqs.(2) with values of C^0_{11}, C^0_{12} and C^0_{44} obtained from the SMA potential.

the following constants C_{ij} are not null and plotted in Fig. 1, in the case of Cu and Au.:

$$\begin{aligned}
&C_{11} = C_{22} = \frac{1}{2}\left(C^0_{11} + C^0_{12} + 2C^0_{44}\right), \quad C_{12} = \frac{1}{6}\left(C^0_{11} + 5C^0_{12} - 2C^0_{44}\right), \quad C_{13} = C_{23} = \frac{1}{3}\left(C^0_{11} + 2C^0_{12} - 2C^0_{44}\right),\\
&C_{33} = \frac{1}{3}\left(C^0_{11} + 2C^0_{12} + 4C^0_{44}\right), \quad C_{44} = C_{55} = \frac{1}{3}\left(C^0_{11} - C^0_{12} + C^0_{44}\right), \quad C_{66} = \frac{1}{6}\left(C^0_{11} - C^0_{12} + 4C^0_{44}\right)\\
&C_{14} = -C_{24} = C_{56} = \frac{\sqrt{2}}{6}\left(C^0_{11} - C^0_{12} - 2C^0_{44}\right)\cos 3\Theta, \quad C_{15} = -C_{25} = -C_{46} = \frac{\sqrt{2}}{6}\left(C^0_{11} - C^0_{12} - 2C^0_{44}\right)\sin 3\Theta
\end{aligned} \tag{2}$$

where C^0_{11}, C^0_{12} and C^0_{44} are the usual three independent elastic constants defined for a cubic crystal and where for $\Theta = 0$, $\mathbf{e}_R$ is chosen along the $[1\bar{1}0]$ direction.

II. SURFACE ELASTIC PARAMETERS

At the surface, the surface strain energy $\psi^S(\mathbf{E}^S)$ per unit undeformed area depends on the second order elastic constants C_{ij}^S where i and j range over the values 2,3 and 4 in the Voigt's convention. Surface strain $\mathbf{E}^S$ changes the 3 components S_i^S of the symmetric surface stress $\mathbf{S}^S$ (in linear surface elasticity) according to

$$S_i^S = S_i^{S,0} + C_{ij}^S E_j^S \tag{3}$$

where $S_2^{S,0} = S_{\Theta\Theta}^{S,0}$, $S_3^{S,0} = S_{ZZ}^{S,0}$ and $S_4^{S,0} = S_{\Theta Z}^{S,0}$ are the 3 surface stress components at $\mathbf{E}^S = \mathbf{0}$.

To calculate $S_i^{S,0}$ and C_{ij}^S as a function of Θ for an $\langle 111 \rangle$ oriented wire we adopt the method described in Ref [2] where we construct and then deform slabs whose surface initially exhibits a structure similar to that encountered locally on the lateral surface of a $\langle 111 \rangle$ wire with circular cross-section. Using molecular statics calculations with the SMA potential, we can then estimate the anisotropy of the surface parameters $S_i^{S,0}$ and C_{ij}^S. Their values obtained for copper and for gold are gathered below in Figs. 2 and 3.

A. $S_i^{S,0}$ and C_{ij}^S at the surface of $\langle 111 \rangle$ circular wire

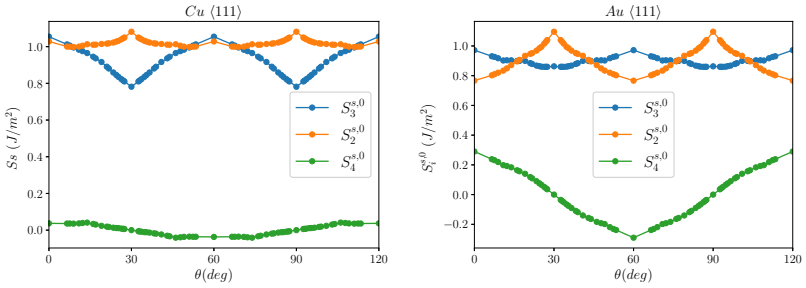

FIG. 2. Calculations from different slabs of the surface parameters $S_i^{S,0}$ as a function of the azimuth Θ for the various surface structures and orientations found around a $\langle 111 \rangle$ circular copper wire (on the left) and around a $\langle 111 \rangle$ circular gold wire (on the right). The particularity of the $\langle 111 \rangle$ wire is that it has a surface shear component $S_4^{S,0} = S_{\Theta Z}^{S,0}$ that varies with Θ. Note that the amplitude of $S_4^{S,0}$ is 7 times higher in the case of Au than in the case of Cu.

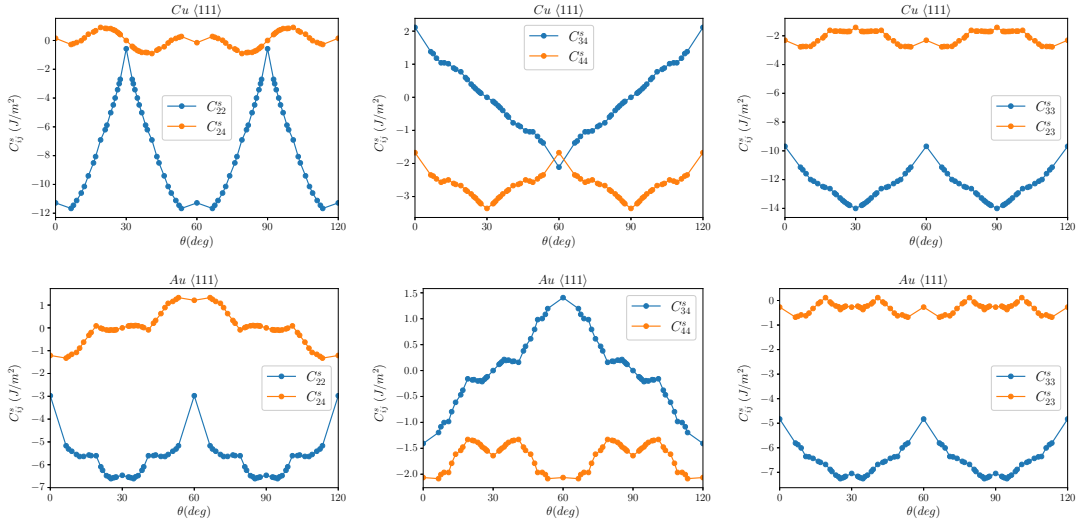

FIG. 3. Calculations from different deformed slabs of the surface elastic constants C_{ij}^S as a function of Θ for the surfaces found around a $\langle 111 \rangle$ circular wire. The first line is obtained for Cu and the second for Au.

B. Expressions of the deformation state of the wire characterized by u_0, w_0 and $g(R,\Theta)$

In the framework of our simplified model where the average radial deformation u_0 is supposed to be independent of R and Θ, it is possible to estimate u_0 and w_0 as a function of the radius of the wire R_0 and to show that the warp function $g(R,\Theta)$ does not depend on u_0 and w_0 for a $\langle 111 \rangle$ wire.

For this purpose, it is in principle necessary to start from the expression of the *first* Piola-Kirchhoff stress tensor $\mathbf{P}$ which, knowing the deformation gradient tensor field $\mathbf{F}$, can be written in our case :

$$\mathbf{P} = \begin{pmatrix} S_{RR} & S_{R\Theta} & S_{RZ} \\ S_{R\Theta} & S_{\Theta\Theta} & S_{\Theta Z} \\ (F_{zR}S_{RR} + F_{z\Theta}S_{R\Theta} + S_{RZ}) & (F_{zR}S_{R\Theta} + F_{z\Theta}S_{\Theta\Theta} + S_{\Theta Z}) & (F_{zR}S_{RZ} + F_{z\Theta}S_{\Theta Z} + S_{ZZ}) \end{pmatrix}$$

However, the terms weighted by F_{zR} and $F_{z\Theta}$ can be safely ignored as long as the warp remains moderate, $\mathbf{P}$ then becomes equal to $\mathbf{S}$:

$$\mathbf{P} \approx \mathbf{S} = \begin{pmatrix} S_{RR} & S_{R\Theta} & S_{RZ} \\ S_{R\Theta} & S_{\Theta\Theta} & S_{\Theta Z} \\ S_{RZ} & S_{\Theta Z} & S_{ZZ} \end{pmatrix}$$

with

$$\begin{aligned} S_{RR} &= C_{11}u_0 + C_{12}u_0 + C_{13}w_0 + C_{14}g'_\Theta/R + C_{15}g'_R \\ S_{\Theta\Theta} &= C_{12}u_0 + C_{22}u_0 + C_{23}w_0 + C_{24}g'_\Theta/R + C_{25}g'_R \\ S_{ZZ} &= C_{13}u_0 + C_{23}u_0 + C_{33}w_0 \\ S_{\Theta Z} &= C_{14}u_0 + C_{24}u_0 + C_{44}g'_\Theta/R \\ S_{RZ} &= C_{15}u_0 + C_{25}u_0 + C_{55}g'_R \\ S_{R\Theta} &= C_{46}g'_\Theta/R + C_{56}g'_R \end{aligned} \tag{4}$$

One can get a first relation that link u_0 to w_0 by considering the Gurtin-Murdoch condition $\mathbf{P}.\mathbf{e}_R - \mathrm{Div}^S\mathbf{P}^S = \mathbf{0}$ imposed on the component S_{RR} at the surface (denoted by $S_{RR}|_{R=R_0}$) :

$$S_{RR}|_{R=R_0} = -\frac{S^S_{\Theta\Theta}}{R_0} \tag{5}$$

with $S^S_{\Theta\Theta} = S^{S,0}_{\Theta\Theta} + C^S_{22}u_0 + C^S_{23}w_0 + C^S_{24}g'_\Theta(R_0)/R_0$

The Gurtin-Murdoch condition is a local relation, but since we are interested here only in the mean value of the radial strain u_0, we consider only the mean values (denoted $\overline{A} = \frac{1}{2\pi}\int_0^{2\pi} A d\Theta$) of the surface parameters in Eq.(5) and replace $g(R_0)$ by its mean value $\overline{g(R_0)}$. Since this latter is null, we find :

$$(C_{11} + C_{12} + \frac{\overline{C^S_{22}}}{R_0})u_0 + (C_{13} + \frac{\overline{C^S_{23}}}{R_0})w_0 = -\frac{\overline{S^{S,0}_{\Theta\Theta}}}{R_0} \tag{6}$$

The second relation between u_0 and w_0 is obtained from the condition which ensures that the wire is free to relax along Z i.e., $\iint_S P_{zZ}dA + \int_{\partial S} P^S_{zZ}dL = 0$, leading in our case to

$$\int_0^{2\pi}\int_0^{R_0} S_{ZZ}RdRd\Theta + R_0\int_0^{2\pi} S^S_{ZZ}d\Theta = 0 \tag{7}$$

with $S^S_{ZZ} = S^{S,0}_{ZZ} + C^S_{23}u_0 + C^S_{33}w_0 + C^S_{43}g'_\Theta(R_0)/R_0$. Noting that $\overline{g(R_0)}$ is null, we find :

$$(2C_{13} + 2\frac{\overline{C^S_{23}}}{R_0})u_0 + (C_{33} + 2\frac{\overline{C^S_{33}}}{R_0})w_0 = -2\frac{\overline{S^{S,0}_{ZZ}}}{R_0} \tag{8}$$

Finally, from Eqs. (6) and (8), one obtains u_0 and w_0 as a function of R_0 :

$$u_0 = \frac{1}{R_0}\frac{2(C_{13} + \frac{\overline{C^S_{23}}}{R_0})\overline{S^{S,0}_{ZZ}} - (C_{33} + 2\frac{\overline{C^S_{33}}}{R_0})\overline{S^{S,0}_{\Theta\Theta}}}{(C_{11} + C_{12} + \frac{\overline{C^S_{22}}}{R_0})(C_{33} + 2\frac{\overline{C^S_{33}}}{R_0}) - 2(C_{13} + \frac{\overline{C^S_{23}}}{R_0})(C_{13} + \frac{\overline{C^S_{23}}}{R_0})} \tag{9}$$

$$w_0 = \frac{2}{R_0}\frac{(C_{13} + \frac{\overline{C^S_{23}}}{R_0})\overline{S^{S,0}_{\Theta\Theta}} - (C_{11} + C_{12} + \frac{C^S_{22}}{R_0})\overline{S^{S,0}_{ZZ}}}{(C_{11} + C_{12} + \frac{\overline{C^S_{22}}}{R_0})(C_{33} + 2\frac{\overline{C^S_{33}}}{R_0}) - 2(C_{13} + \frac{\overline{C^S_{23}}}{R_0})(C_{13} + \frac{\overline{C^S_{23}}}{R_0})} \tag{10}$$

Using Table (I), u_0 and w_0 expressed in Eqs.(9) and (10) are compared in Fig. 4 to their values obtained from MS simulations of various $\langle 111 \rangle$ wires with circular cross-section.

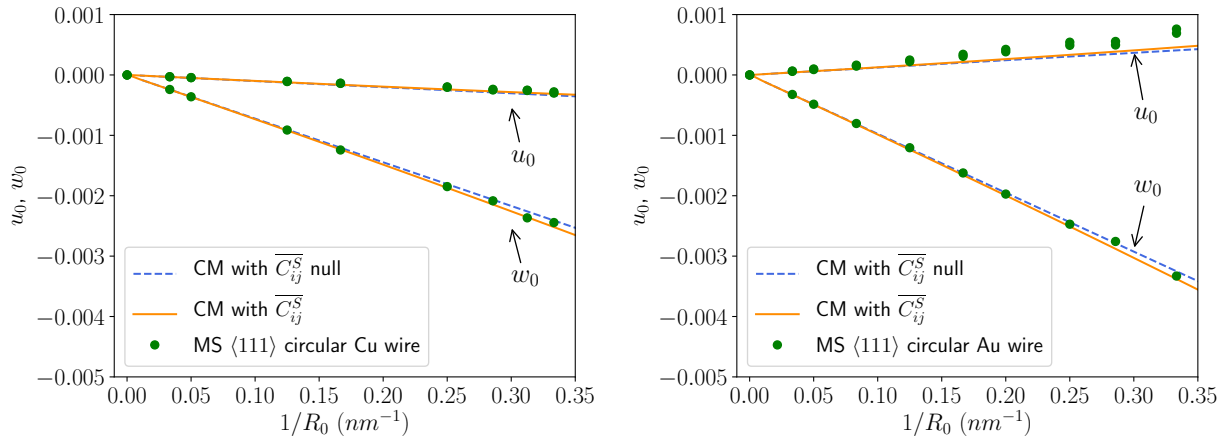

FIG. 4. Influence of the surface elastic constants C_{ij}^S on the axial contraction w_0 and the radial deformation u_0 in Cu (on the left) and Au (on the right) ⟨111⟩ nanowires of circular cross section given by Eqs.(9) and (10) resulting from the continuum model (CM). The elastic constants are taken from the Table I. The CM curves are compared to the results of molecular statics simulations (MS) performed on various ⟨111⟩ nanowires of different radii R_0. The MS value of the radial deformation u_0 is calculated by averaging the radial displacement u_R of atoms located at a distance $R_0/2 < R < 2R_0/3$ from the center so that $u_0 = \frac{1}{\pi R_0}\int_0^{2\pi} u_R d\Theta$.

	C_{11}^0	C_{12}^0	C_{44}^0	$\overline{S_{\Theta\Theta}^{S,0}}$	$\overline{S_{ZZ}^{S,0}}$	$\overline{C_{22}^S}$	$\overline{C_{23}^S}$	$\overline{C_{33}^S}$
Cu ⟨111⟩	169 GPa	127 GPa	69 GPa	1.02 J/m^2	0.94 J/m^2	-8.09 J/m^2	-2.17 J/m^2	-12.196 J/m^2
Au ⟨111⟩	184 GPa	154 GPa	42 GPa	0.89 J/m^2	0.90 J/m^2	-5.51 J/m^2	-0.30 J/m^2	-6.38 J/m^2

TABLE I. Values of the bulk elastic constants C_{11}^0, C_{12}^0 and C_{44}^0 given by the SMA potential for Cu and Au are recalled. The average values of the surface elastic parameters which appear in Eqs. (9) and (10) are calculated from Figs. 2 and 3.

It should be remembered, however, that this comparison must be read with care. Indeed, if w_0 is observed in the simulations as being constant over the entire wire cross-section, this is not the case for $u_0 = (r - R)/R$, which varies with Θ and R. In Fig. 4, to extract u_0 from the simulations, an average value over Θ is calculated, showing that this average value changes little if it is performed far from the surface for $R = R_0/2$ or for $R = 2R_0/3$, for example. From Fig. 4, we can see that Eqs. (9) and (10) remain fairly reliable for predicting w_0 and u_0 for ⟨111⟩ oriented wires. However, taking surface elastic constants into account does not significantly improve the description, unlike in the case of ⟨100⟩ copper wire previously studied in Ref [2]. For the ⟨111⟩ wires considered in this work, the main interest of the model is to be able to capture the change in sign of u_0 depending on the metal considered. We can see that the contraction of the wire along its axis is not systematically accompanied by radial expansion (u_0 positive). This is the case of copper, for which we observe a radial contraction (u_0 is negative) that cannot be explained simply with isotropic elasticity. Indeed, according to Ref [3], this latter predicts a ratio $\frac{u_0}{w_0} = \frac{3\nu-1}{2(\nu-1)}$ where ν represents the Poisson's ratio that is equal to 0.34 for copper [4]. Using Eqs. (9) and (10), this aspect is clarified in the Letter and the ratio u_0/w_0 is estimated as a function of the C_{11}^0, C_{12}^0 and C_{44}^0 more accurately.

The last point discussed in this section is the expression of the warp function $g(R, \Theta)$ for a ⟨111⟩ wire. The latter can be easily established if we consider u_0 to be independent of R and Θ.

Let's first consider the third equilibrium equation given by $\mathrm{Div}\mathbf{P} = \mathbf{0}$:

$$\frac{\partial P_{zR}}{\partial R} + \frac{P_{zR}}{R} + \frac{1}{R}\frac{\partial P_{z\Theta}}{\partial \Theta} + \frac{\partial P_{zZ}}{\partial Z} = 0 \tag{11}$$

Noting that P_{zZ} does not vary with Z and assuming that $\mathbf{P} \approx \mathbf{S}$, we have :

$$\frac{\partial S_{RZ}}{\partial R} + \frac{S_{RZ}}{R} + \frac{1}{R}\frac{\partial S_{\Theta Z}}{\partial \Theta} = 0 \tag{12}$$

where S_{RZ} and $S_{\Theta Z}$ are given by Eqs. (4). Considering the symmetry properties of the C_{ij} given by Eqs.(2) for the

$\langle 111 \rangle$ zone axis, and the expressions of S_{RZ} and $S_{\Theta Z}$ in Eqs.(4), Eq.(12) leads to the following condition on $g(R,\Theta)$:

$$g''_R + \frac{g'_R}{R} + \frac{g''_\Theta}{R^2} = 0 \tag{13}$$

where $g''_R = \partial g'_R/\partial R$, $g'_R = \partial g/\partial R$ and $g''_\Theta = \partial^2 g/\partial \Theta^2$.

Taking into account the threefold symmetry of the boundary conditions on the lateral surface of the nanowire, we seek an expression of $g(R,\Theta)$, solution of Eq.(13), having the following form:

$$g(R,\Theta) = \sum_{N=1}^{\infty} g_N R^{3N} \sin 3N\Theta \tag{14}$$

where the g_N coefficients are determined in this work by applying the Gurtin-Murdoch surface conditions. From these latter we have :

$$P_{zR}\big|_{R=R_0} = \frac{1}{R_0}\frac{\partial P^S_{z\Theta}}{\partial \Theta} + \frac{\partial P^S_{zZ}}{\partial Z} \tag{15}$$

which in the present case takes the simple form :

$$\begin{aligned} &\left(F_{zR}S_{RR} + F_{z\Theta}S_{R\Theta} + (1+w_0)S_{RZ}\right)\big|_{R=R_0} \\ &\quad = \frac{1}{R_0}\frac{\partial}{\partial \Theta}\left((1+w_0)S^S_{\Theta Z} + F^S_{z\Theta}S^S_{\Theta\Theta}\right) \end{aligned} \tag{16}$$

where

$$\begin{aligned} F_{zR}S_{RR} &= g'_R\left(C_{11}u_0 + C_{12}u_0 + C_{13}w_0 + C_{14}\frac{g'_\Theta}{R} + C_{15}g'_R\right), \\ F_{z\Theta}S_{R\Theta} &= \frac{g'_\Theta}{R}(C_{46}\frac{g'_\Theta}{R} + C_{56}g'_R), \\ S_{RZ} &= C_{55}g'_R, \\ S^S_{\Theta Z} &= S^{S,0}_{\Theta Z} + C^S_{24}u_0 + C^S_{34}w_0 + C^S_{44}\frac{g'_\Theta(R_0)}{R_0}, \\ F^S_{z\Theta}S^S_{\Theta\Theta} &= \frac{g'_\Theta(R_0)}{R_0}\left(S^{S,0}_{\Theta\Theta} + C^S_{22}u_0 + C^S_{23}w_0 + C^S_{24}\frac{g'_\Theta(R_0)}{R_0}\right) \end{aligned} \tag{17}$$

Neglecting terms involving products between u_0, w_0, $g'_\Theta(R_0)$ and $g'_R(R_0)$, we obtain :

$$\begin{aligned} &g'_R(R_0,\Theta) = \\ &\quad \frac{1}{R_0 C_{55}}\frac{\partial}{\partial \Theta}\left(S^{S,0}_{\Theta Z} + C^S_{24}u_0 + C^S_{34}w_0 + (S^{S,0}_{\Theta\Theta} + C^S_{44})\frac{g'_\Theta(R_0)}{R_0}\right) \end{aligned} \tag{18}$$

which can be further simplified by considering u_0, w_0, $g'_\Theta(R_0)/R_0$ sufficiently small so that $S^{S,0}_{\Theta Z}$ is the dominant term.

$$g'_R(R_0,\Theta) = \frac{1}{R_0 C_{55}}\frac{\partial S^{S,0}_{\Theta Z}}{\partial \Theta} \tag{19}$$

where $C_{55} = \frac{1}{3}\left(C^0_{11} - C^0_{12} + C^0_{44}\right)$. To check that the simplification from Eq. (18) to Eq. (19) is justified for the Cu and Au cases considered in this work, we plot in Fig. 5 the terms neglected in Eq. (18) for two different radii.

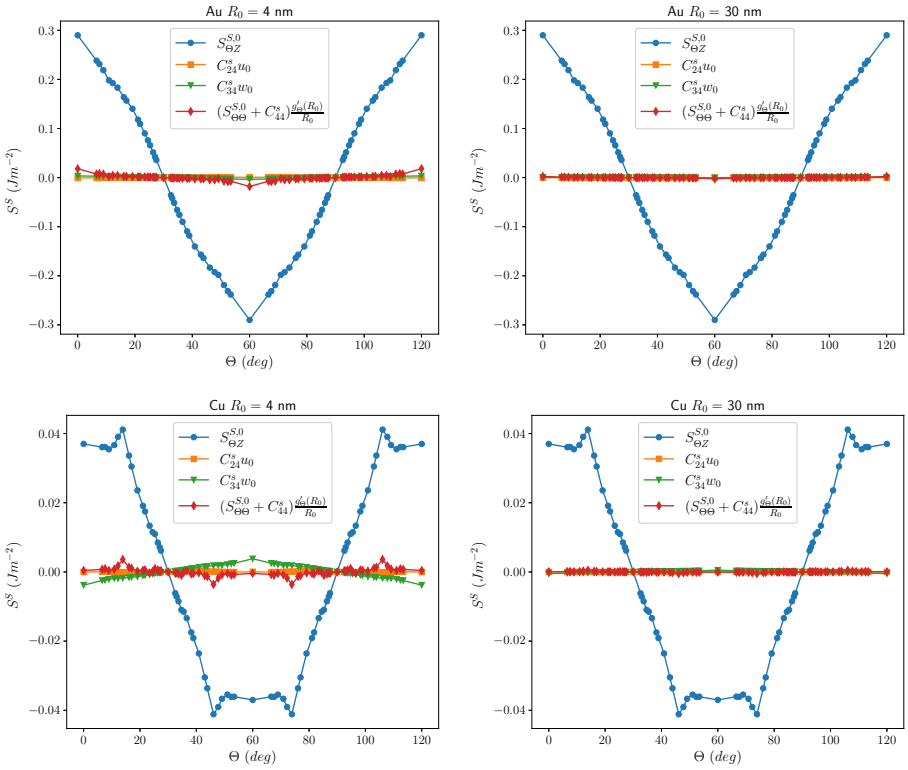

FIG. 5. $S^{S,0}_{\Theta Z}$ is found to be the dominant term in Eq.(18). This is verified numerically here by plotting the terms $S^{S,0}_{\Theta Z}$, $C^S_{24}u_0$, $C^S_{34}w_0$, and $(S^{S,0}_{\Theta\Theta} + C^S_{44})\frac{g'_\Theta(R_0)}{R_0}$ which appear in Eq.(18) as a function of the azimut Θ from MS simulations performed on both Cu and Au nanowires of radius $R_0 = 4$nm and $R_0 = 30$nm.

C. $\langle 111 \rangle$ Cu nanowire with circular cross-section

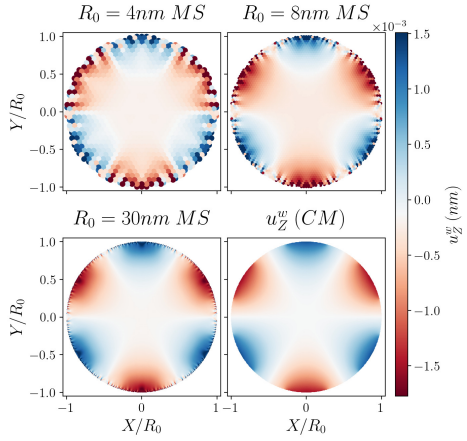

FIG. 6. Warp displacement fields u^w_Z (nm) in $\langle 111 \rangle$ Cu nanowires of circular cross section (for different radii : $R_0 = 4$, 8 and 30 nm). Comparison of the warp $u^w_Z(MS)$ observed in the atomistic simulations with $u^w_Z(CM)$ predicted by our continuum model where the g_N coefficients in Eq.(14) are determined from the Fourier analysis of $S^{S,0}_{\Theta Z}$ shown in Fig.2.

D. ⟨111⟩ Cu nanowire with an hexagonal cross-section presenting {112} surfaces

Another case that deserves further study is that of copper nanowires with an hexagonal cross-section, but whose faces are {112} oriented. We have shown that the S_4^S of these surfaces is null, so the warp can again only be due to edge effects. We discuss this case here, where a guess of the S_4^S function based on the observation of the S_4 value per atom enables us to qualitatively reproduce in Fig. 7 the warp observed in the simulations.

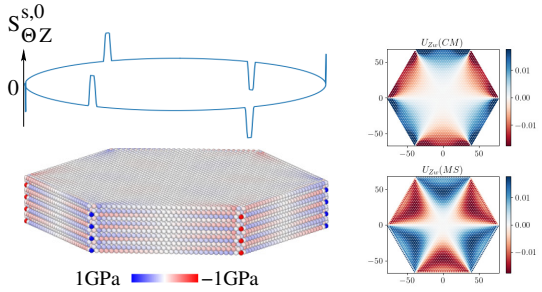

FIG. 7. Warp displacement fields u_Z^w (nm) in ⟨111⟩ Cu nanowires of hexagonal cross section with planar {112} surfaces. Comparison of the warp $u_Z^w(MS)$ observed in the atomistic simulations with $u_Z^w(CM)$ predicted by our continuum model where the g_N coefficients in Eq.(14) are determined from the Fourier analysis of a $S^{S,0}_{\Theta Z}$ function chosen to roughly reproduce the fact that only atoms located at the edges have non-zero $S_{\Theta Z}$ values, as shown here on the simulated wire slice.

E. ⟨111⟩ Au nanowires with a triangular cross-section presenting {110} surfaces : a remarkable case where S_4^S induces the twist of the wire

As an extension to this work, it would be interesting to study other cross-sections in detail. Indeed, it is possible to envisage situations where the surface shear stress $S_4^{S,0}$ is such that the resulting torque is non-zero. This is a particularly interesting case, since it should generate a torsion of the wire. Such a situation would be encountered for the case of a triangular cross-section which presents only one of the two types of {110} surfaces (and therefore having the same $S_4^{S,0}$ value). To illustrate this point, we show in Fig. 8 the results of MS simulations for free ⟨111⟩ wires with the two types of triangular cross-sections. At equilibrium, they do indeed exhibit a twist whose direction can be ascribed to the sign of surface shear stress $S_4^{S,0}$.

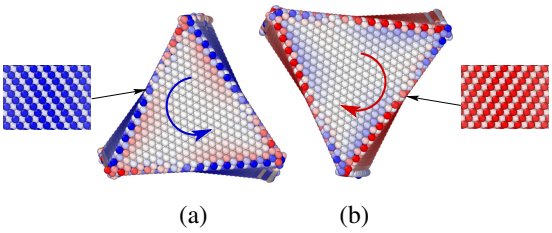

FIG. 8. MS simulations of free [111] wires with a triangular cross-section (top view). The orientations of the lateral surfaces are (a) : $(\bar{1}10)$, $(0\bar{1}1)$, $(10\bar{1})$ with $S_4^{S,0} \approx$ - 0.3 J.m^{-2} , and (b) : $(1\bar{1}0)$, $(01\bar{1})$ et $(\bar{1}01)$ with $S_4^{S,0} \approx +$ 0.3 J.m^{-2}. At equilibrium, the wires are twisted according to the sign of the torque induced by the surface shear stress $S_4^{S,0}$ of the {110} surfaces.

[1] K. Brugger, Thermodynamic definition of higher order elastic coefficients, Phys. Rev. **133**, A1611 (1964).
[2] J.-M. Roussel and M. Gailhanou, Warping caused by surface elasticity in a nanowire under torsion, Phys. Rev. B **107**, 094110 (2023).
[3] A. Roy, S. Kundu, K. Müller, A. Rosenauer, S. Singh, P. Pant, M. P. Gururajan, P. Kumar, J. Weissmüller, A. K. Singh, and N. Ravishankar, Wrinkling of atomic planes in ultrathin au nanowires, Nano Letters **14**, 4859 (2014).
[4] L. Freund and S. Suresh, *Thin Film Materials: Stress, Defect Formation and Surface Evolution* (Cambridge University Press, 2004).